Published in final edited form as:
Nature. 2013 June 20; 498(7454): 325–331. doi:10.1038/nature12204.

Genetic screens reveal RAS/MAPK/MSK1 modulate ataxin 1 protein levels and toxicity in SCA1

Jeehye Park[#1,2,3], **Ismael Al-Ramahi**[#1,2], **Qiumin Tan**[1,2,3], **Nissa Mollema**[4,5], **Javier R. Diaz-Garcia**[1,2], **Tatiana Gallego-Flores**[1,2], **Hsiang-Chih Lu**[2,6], **Sarita Lagalwar**[4,5], **Lisa Duvick**[4,5], **Hyojin Kang**[1,2,†], **Yoontae Lee**[1,2,3,†], **Paymaan Jafar-Nejad**[1,2], **Layal S. Sayegh**[1,2], **Ronald Richman**[1,2,3], **Xiuyun Liu**[1,2,3], **Yan Gao**[1,2], **Chad A. Shaw**[1], **J. Simon C. Arthur**[7], **Harry T. Orr**[4,5], **Thomas F. Westbrook**[1,6,8], **Juan Botas**[1,2], and **Huda Y. Zoghbi**[1,2,3,6]

[1]Department of Molecular and Human Genetics, Baylor College of Medicine, Houston, Texas 77030, USA.

[2]Jan and Dan Duncan Neurological Research Institute at Texas Children's Hospital, Houston, Texas 77030, USA.

[3]Howard Hughes Medical Institute, Baylor College of Medicine, Houston, Texas 77030, USA.

[4]Institute for Translational Neuroscience, University of Minnesota, Minneapolis, Minnesota 55455, USA.

[5]Department of Laboratory Medicine and Pathology, University of Minnesota, Minneapolis, Minnesota 55455, USA.

[6]Program in Developmental Biology, Baylor College of Medicine, Houston, Texas 77030, USA.

[7]MRC Protein Phosphorylation Unit, School of Life Sciences, University of Dundee, Dundee, DD1 5EH, UK.

[8]Verna and Marrs McLean Department of Biochemistry and Molecular Biology, Baylor College of Medicine, Houston, Texas 77030, USA.

[#] These authors contributed equally to this work.

Abstract

Many neurodegenerative disorders such as Alzheimer's, Parkinson's and polyglutamine diseases share a common pathogenic mechanism: the abnormal accumulation of disease-causing proteins, due to either the mutant protein's resistance to degradation or overexpression of the wild-type

Correspondence and requests for materials should be addressed to H.T.O. (orrxx002@umn.edu), T.F.W. (thomasw@bcm.edu), J.B. (jbotas@bcm.edu) or H.Y.Z. (hzoghbi@bcm.edu)..

[†]Present addresses: Supercomputing Center, Korea Institute of Science and Technology Information, Daejeon, 305-806, South Korea (H.K.); Department of Life Science, Pohang University of Science and Technology, Pohang, Kyungbuk 790-784, South Korea (Y.L.).

Supplementary Information is available in the online version of the paper.

Author Contributions J.P., I.A.-R., Q.T., N.M., H.T.O., T.F.W., J.B. and H.Y.Z. designed the experiments. J.P., I.A.-R., Q.T., N.M., J.R.D.-G., T.G.-F., H.-C.L., S.L., L.D., H.K., Y.L., P.J.-N., L.S.S., R.R., X.L. and Y.G. performed the research. J.P., I.A.-R., Q.T., N.M., J.R.D.-G., T.G.-F., H.-C.L., S.L., L.D., H.K., Y.L., P.J.-N., C.A.S., J.S.C.A., H.T.O., T.F.W., J.B. and H.Y.Z. analysed and interpreted the data. J.P., I.A.-R., H.T.O., T.F.W., J.B. and H.Y.Z. wrote and edited the paper.

Author Information Reprints and permissions information is available at www.nature.com/reprints. The authors declare no competing financial interests. Readers are welcome to comment on the online version of the paper.

protein. We developed a strategy to identify therapeutic entry points for such neurodegenerative disorders by screening for genetic networks that influence the levels of disease-driving proteins. We applied this approach, which integrates parallel cell-based and *Drosophila* genetic screens, to spinocerebellar ataxia type 1 (SCA1), a disease caused by expansion of a polyglutamine tract in ataxin 1 (ATXN1). Our approach revealed that downregulation of several components of the RAS–MAPK–MSK1 pathway decreases ATXN1 levels and suppresses neurodegeneration in *Drosophila* and mice. Importantly, pharmacologic inhibitors of components of this pathway also decrease ATXN1 levels, suggesting that these components represent new therapeutic targets in mitigating SCA1. Collectively, these data reveal new therapeutic entry points for SCA1 and provide a proof-of-principle for tackling other classes of intractable neurodegenerative diseases.

The increasing prevalence of neurodegenerative diseases such as Alzheimer's disease and Parkinson's disease in the ageing population is one of our most pressing public health issues[1,2]. There is no disease-modifying treatment for most of these disorders; those therapies that do exist target the late stages of disease, when pathogenesis is already advanced and the symptomatic relief is partial and short-lived[3,4]. It would clearly be preferable to either delay the onset of symptoms, slow disease progression or reverse the course of the disease, but to do this probably requires us to address earlier stages of pathogenesis.

Fortunately, two decades of research on inherited neurodegenerative diseases (Huntington's disease, the spinocerebellar ataxias and inherited forms of Alzheimer's disease and Parkinson's disease) have revealed certain pathogenic commonalities at the molecular level[5]. For instance, although the respective disease-causing proteins (HTT, ataxins, APP and α-synuclein) and neuronal populations vulnerable to their toxicity are distinct in each disorder[6–8], each of these diseases involves the toxic accumulation of the mutant protein; in some cases too much of the wild-type protein is also toxic[9–11]. Importantly, animal models have shown that decreasing the accumulation of the normal or mutant proteins, usually by genetic manipulation, can reverse disease phenotypes[12–18]. We therefore set out to identify druggable targets that modulate the level of a neurodegenerative disease-causing protein: glutamine-expanded ATXN1, which is mutated in SCA1.

To exploit the unbiased, functional nature of genetic screens and compensate for the weaknesses inherent in any given model system, we developed a cross-species strategy: complementary forward genetic screens that targeted the levels of glutamine-expanded human ATXN1 in a SCA1 *Drosophila* model and in a human cell model for SCA1. We chose to use modulation of ATXN1 levels as a proof-of-principle for this strategy for three reasons: (1) the severity of neurodegeneration in SCA1 correlates with the levels of the mutant ATXN1 protein; (2) overexpression of wild-type ATXN1 leads to neurodegeneration; and (3) the pathogenic mechanisms underlying SCA1 are well characterized[19]. Our genetic screening approach revealed that multiple components of the RAS–MAPK–MSK1 pathway influence ATXN1 levels in *Drosophila* and human cells. We then validated these results using SCA1 mouse models and further found that pharmacologic targeting of this pathway also reduces ATXN1 levels.

Strategy to identify regulators of ATXN1 levels

To identify regulators of ATXN1 levels in human cells of neural lineage, we engineered a human medulloblastoma-derived cell line with a transgene encoding a glutamine-expanded ATXN1 fused with monomeric red fluorescent protein (mRFP–ATXN1(82Q)). To distinguish modifiers regulating ATXN1 protein levels from those affecting transgene transcription, we placed an internal ribosomal entry site (IRES) followed by yellow fluorescent protein (YFP) downstream of the ATXN1 fusion protein (mRFP–ATXN1(82Q)–IRES–YFP). The ratio of mRFP to YFP fluorescence by flow cytometric analysis thus serves as a read-out for genes that regulate mRFP– ATXN1(82Q) protein levels while controlling for fluctuations in transcription of the transgene (Fig. 1a).

We focused on interrogating human kinases, because (1) phosphorylation is crucial to ATXN1 toxicity[20]; and (2) many kinases are targeted (or amenable to targeting by) pharmacologic agents[21]. We used this cell system to test individually the effects of short interfering RNAs (siRNAs) targeting every known human kinase and kinase-like gene (1,908 siRNAs, 636 genes; tests performed in triplicate) on ATXN1 levels. We selected for further study 181 siRNAs that reduced the ratio of mRFP to YFP fluorescence by two standard deviations from the screen-wide mean (Fig. 1b). siRNAs from these primary hits were transfected independently in ATXN1(82Q) cells for confirmation and were tested in parallel with a control reporter line (cells encoding mRFP–IRES–YFP lacking the ATXN1 fusion) to eliminate false-positive hits that targeted mRFP. These analyses validated 50 siRNA candidates (corresponding to 45 genes) that reduce ATXN1(82Q) levels (Supplementary Table 1).

In parallel, we performed a genetic screen in a *Drosophila* SCA1 model expressing human ATXN1(82Q) that develops an external eye phenotype in response to ATXN1 toxicity[22] (Fig. 1c). We screened a total of 704 alleles (including inducible short hairpin RNAs (shRNAs) and loss-of-function mutations) corresponding to 337 kinase-encoding *Drosophila* genes for those that would modulate mutant ATXN1 levels. We then performed retinal sections to determine whether these modulators of the external eye phenotype also improved photoreceptor integrity. The morphological and histological phenotype assessment yielded 51 alleles (corresponding to 49 genes) that suppressed ATXN1(82Q) toxicity *in vivo* (Supplementary Table 2).

These *Drosophila*- and human-cell-based screens revealed ten modifier genes that reduce both ATXN1 levels and ATXN1-induced toxicity (*IGF1R*, *ULK3*, *WNK4*, *BUB1*, *MSK1* (also known as *RPS6KA5*), *MEK2* (also known as *MAP2K2*), *MEK3* (also known as *MAP2K3*), *MEK6* (also known as *MAP2K6*), *ERK1* (also known as *MAPK3*) and *ERK2* (also known as *MAPK1*)) and which correspond to eight modifiers in *Drosophila* (*CG3837*, *CG8866*, *CG7177*, *BubR1*, *JIL-1*, *Dsor1*, *lic* and *rl*) (Figs 1c, d, 2a–c and Supplementary Fig. 1). We selected these genes for further characterization.

Reducing MAPK signalling decreases ATXN1

Network analysis of the hits from human cells and *Drosophila* revealed that the MAPK cascade is the most enriched pathway in each screen (Supplementary Table 3). In addition,

analysis of the ten common genes shows that the MAPK cascade is the most highly represented signalling pathway. In fact, six of the ten shared hits (ERK1, ERK2, MEK2, MEK3, MEK6 and MSK1) are canonical components of this pathway, and WNK4 and IGF1R are known to regulate it[23–25] (Fig. 2e, Supplementary Table 4 and Supplementary Fig. 1d). This pathway is a component of a cell-signalling cascade that also includes RAS, RAF and MEK and that can be activated by a variety of mitogens, growth factors and receptor tyrosine kinases[26,27] (Supplementary Fig. 1d). To validate the effects of the MAPK pathway hits in the central nervous system (CNS) of an intact animal, we used a motor performance assay that measures climbing ability in fruitflies. Expression of ATXN1(82Q) in the *Drosophila* CNS leads to progressive impairment in motor performance[28]. We found that decreased levels of the *Drosophila* homologues of MEK (DSOR1), ERK1/2 (RL) and MSK1 (JIL-1) suppressed ATXN1(82Q)-induced motor deficits and improved lifespan in ATXN1(82Q) flies (Fig. 2d).

We next sought to determine whether other upstream components of the MAPK pathway modulate ATXN1 toxicity. We found that decreased levels of the *Drosophila* homologues of farnesyltransferase (FNTB), GRB2, SOS, HRAS, RRAS and RAF suppress the ATXN1(82Q)-induced external eye phenotype as well as photoreceptor degeneration (Fig. 3a and Supplementary Fig. 2a, b). Decreasing the levels of the *Drosophila* homologues of FNTA, SOS, HRAS and RAF improved the ATXN1(82Q)-induced motor and lifespan phenotypes (Fig. 3b and Supplementary Fig. 3). In addition, activation of MAPKs via a constitutively active form of *Drosophila* RAS (dRAS-V12) exacerbated the ATXN1(82Q)-induced eye degeneration (Supplementary Fig. 4a).

Prompted by this genetic evidence that the RAS–MAPK–MSK pathway governs ATXN1(82Q)-induced phenotypes, we investigated the ability of this pathway to modulate ATXN1(82Q) protein levels. We found that reducing the levels of *HRAS* and *FNTA* led to a decrease in ATXN1 levels in human cells (Fig. 3c, d, Supplementary Fig. 2c and Supplementary Fig. 5). Furthermore, we confirmed that decreasing the levels of any of the two functionally conserved RAS homologues in *Drosophila* (dRAS and RAS64B) also decreased the levels of ATXN1(82Q) *in vivo* (Fig. 3e). Reducing the levels of the RAS/MAPK genes also decreased ATXN1(30Q) levels in cells and suppressed ATXN1(30Q)-induced toxicity in *Drosophila* (Supplementary Fig. 6).

In summary, the genetic screen in cells and fruit flies unveiled the RAS/MAPK pathway as critical for modulating ATXN1 levels (Fig. 3f).

MSK1 stabilizes ATXN1 by phosphorylating S776

Building on our previous discovery that ATXN1 levels are highly sensitive to phosphorylation at residue S776 (mutation of serine to alanine decreases both ATXN1 stability and toxicity)[20,29], we investigated whether the MAPK pathway kinases (MEK, ERK and MSK1) recovered in our screens phosphorylate ATXN1 at S776. This residue falls within the consensus phosphorylation sequence RXXS that is conserved in ATXN1 homologues (Fig. 4a). Most MAPK proteins are known to prefer PX(S/T)P, so we excluded

MEK and ERK. Instead, we focused on MSK1, which is known to prefer the consensus sequence RXXS[30].

To determine whether MSK1 directly phosphorylates ATXN1 at S776, we conducted *in vitro* kinase assays with purified MSK1 and glutathione-*S*-transferase–ATXN1(82Q) (GST–ATXN1(82Q)). We immunoblotted with anti-phospho-S776 ATXN1 antibody[20] and found that the antibody detected robust phospho-S776 ATXN1 signal upon addition of MSK1 (Fig. 4b). Furthermore, MSK1 can phosphorylate both the mutant GST–ATXN1(82Q) and the wild-type GST–ATXN1(30Q) (Fig. 4b). It is noteworthy that RSK1 (also known as RPS6KA1) and RSK2(also known as RPS6KA3) two other kinases that share the RXXS consensus sequence and are also downstream of the MAPK pathway[30], failed to phosphorylate the S776 site (Supplementary Fig. 7a–c).

We next investigated whether the observed effect of MSK1 on ATXN1 stability is mediated by S776 phosphorylation *in vivo*. We found increased levels of ATXN1(82Q) upon coexpression with Msk1 in Neuro2A cells (Fig. 4c). This increase was dependent on S776 phosphorylation, because Msk1 did not increase the levels of ATXN1(82Q, S776A) (Fig. 4c). We also performed cerebellar fractionation assays from wild-type mouse brains and examined whether Msk1 was enriched in the fractions containing S776 phosphorylation activity. As shown in Supplementary Fig. 8a, Msk1 was enriched in the fractions containing peak S776-phosphorylating activity. To confirm whether endogenous Msk1 from neural lineages contributes to ATXN1 phosphorylation, we immunodepleted Msk1 from mouse cerebellar extracts and found that reduction of Msk1 significantly decreased S776 phosphorylation of bacterially purified ATXN1 compared to non-depleted extracts (Fig. 4d and Supplementary Fig. 7d).

Having established the role of MSK1 in phosphorylating a serine critical for modulating ATXN1 stability, we investigated the effects of MSK1 on ATXN1 level in *Drosophila*. We found that reducing the level of the *Drosophila* homologue of MSK1 decreased the steady-state level of ATXN1(82Q) *in vivo* (Fig. 4e).

In summary, the data from the cell-based screen, biochemical studies and genetic interactions strongly suggest that MSK1 phosphorylates ATXN1 and regulates its stability. Furthermore, we tested whether the components upstream of MSK1 in the MAPK pathway also affect ATXN1 S776 phosphorylation. Western blot analysis showed that knockdown of *RAS*, *FNTA* and *MEK* significantly decreases S776 phosphorylation, whereas constitutive activation of RAS and MEK1 markedly increases its phosphorylation and stability (Supplementary Fig. 4b, c and Supplementary Fig. 5).

Together, these results suggest that the RAS–MAPK–MSK1 pathway regulates ATXN1 stability through S776 phosphorylation.

Inhibition of MAPK pathway decreases ATXN1

Our data indicate that genetic inhibition of the MAPK pathway reduces ATXN1 levels and phenotypes. To evaluate the MAPK pathway as a potential therapeutic target for SCA1, we investigated whether pharmacological inhibition of the MAPK pathway (Fig. 3f) decreases

ATXN1 levels. Treating human cells stably expressing ATXN1(82Q) with PD184352, an MEK1/2 inhibitor[31], or GW5704, a RAF1 inhibitor[32], decreased ATXN1(82Q) levels (Fig. 5a). The MSK1 inhibitors, H89 and Ro-31-8220[33], also decreased the levels of ATXN1(82Q) (Fig. 5a).

To examine this reduction in a more physiologically relevant system, we tested whether inhibiting MAPK or MSK1 signalling affected Atxn1(82Q) abundance in the context of cerebellar slice cultures from SCA1 (82Q) knock-in mice[34]. Western blot analysis (Fig. 5b, c) showed that inhibition of MEK1/2 or MSK1 (by addition of PD184352 and Ro-31-8220, respectively) in cerebellar slice cultures decreased the levels of mutant Atxn1.

Together with the genetic data, these results strongly support the hypothesis that the MAPK/MSK1 pathway regulates ATXN1 levels. These findings also validate the genetic screen strategy and provide evidence that ATXN1 levels can be modulated pharmacologically.

Reducing MSK1 rescues degeneration in SCA1 mice

We next sought to test the genetic interaction between MSK1 and ATXN1 in mice. For this we used *Atxn1(154Q)* knock-in mice (*Atxn1*$^{154Q/+}$), which bear 154 CAG repeats in the endogenous mouse locus and recapitulate many features of human SCA1 (ref. 35). These mice were bred to *Msk1*$^{+/-}$ *Msk2*$^{+/-}$ mice, which show no obvious phenotypes[36,37]. First we analysed whether *Msk1* knockout would decrease Atxn1(154Q) in *Atxn1*$^{154Q/+}$ mice. Indeed, *Atxn1*$^{154Q/+}$ *Msk1*$^{-/-}$ animals presented lower levels of expanded Atxn1 than *Atxn1*$^{154Q/+}$ animals (Fig. 6a, b).

Atxn1$^{154Q/+}$ mice develop a motor phenotype that can be quantified after 9 weeks of age using a rotarod test. *Drosophila* has only one *Msk* gene (*JIL-1*), but mice have two paralogues: *Msk1* and *Msk2*. To account for potential genetic redundancy, we investigated the effect on the Atxn1(154Q)-induced phenotype of decreasing both genes simultaneously. The *Atxn1*$^{154Q/+}$ *Msk1*$^{+/-}$ *Msk2* $^{+/-}$ animals showed significantly better rotarod performance than their *Atxn1*$^{154Q/+}$ littermates ($P = 0.027$, Fig. 6c).

Next, we assessed the potential effect of decreasing Msk on Purkinje cell degeneration. Because Purkinje cell loss takes over 7–8 months to manifest in the *Atxn1*$^{154Q/+}$ mice, we resorted to another SCA1 mouse model that expresses ATXN1(82Q) using the *Pcp2* promoter (B05 transgenic mice) and develops severe Purkinje cell degeneration after 12 weeks[38]. We found that eliminating one copy of mouse *Msk1* partially suppressed this Purkinje cell loss phenotype. Simultaneous elimination of one copy of *Msk1* and *Msk2* (*B05*$^{/+}$ *Msk1*$^{+/-}$ *Msk2*$^{+/-}$) also suppressed Purkinje cell loss (Fig. 6d). Moreover, *B05*$^{/+}$ *Msk1*$^{+/-}$ and *B05*$^{/+}$ *Msk1*$^{+/-}$ *Msk2*$^{+/-}$ mice have improved calbindin immunoreactivity in Purkinje cell dendrites compared to *B05*$^{/+}$ ($P < 0.001$ and $P < 0.01$, respectively). Notably, *B05*$^{/+}$ *Msk1*$^{+/-}$ *Msk2*$^{+/-}$ animals showed decreased levels of ATXN1(82Q) compared to *B05*$^{/+}$ controls **(**Supplementary Fig. 8b).

Discussion

Here we combine cross-species genetic screens and validation in human, mouse and *Drosophila* systems to identify previously unappreciated modulators of the steady-state levels of a neurodegeneration-causing protein. Two key discoveries highlight the power and reliability of this screening strategy. First, several modulators of ATXN1 levels belong to a single pathway, the RAS–MAPK–MSK1 signalling pathway. The functional relationship between the newly identified ATXN1 modulators underscores the validity of the approach and distinguishes these findings from screens done in one system whereby the large number of hits often precludes identifying the true positives and linking them in a functional pathway. Second, the screening approach and subsequent characterization revealed a direct biochemical mechanism governing ATXN1 levels (ATXN1 S776 phosphorylation by MSK1) as well as upstream regulators of ATXN1 abundance. The identification of direct (MSK1) and upstream (RAS and MAPK) regulators of ATXN1 levels provides several entry points for developing strategies for therapeutic intervention for SCA1.

Identifying multiple targets that can decrease disease protein levels is important for several reasons. First, the discovery of multiple therapeutic entry points counterbalances the frequent attrition of therapeutic targets during drug development. Second, the discovery of multiple targets enables the development of combination strategies (via multiple inhibitors or inhibitors with activity towards multiple targets[39]) to balance symptom mitigation and side effects. We note that, in the case of ATXN1, S776 can be phosphorylated by PKA[29]. The discovery that MSK1 also phosphorylates ATXN1 at S776 raises the possibility that mild-to-modest inhibition of both kinases might be more effective than severe inhibition of either. Of course, the availability of several additional modulators of ATXN1 levels in the RAS–MAPK–MSK1 pathway now provides further opportunity to explore the development of combination therapeutics.

Previous efforts aimed at developing unbiased screens for the discovery of therapeutic targets for neurodegenerative diseases have focused on protein aggregation or suppression of neuronal cell death[40]. The strategy we used in this study focuses on targeting an earlier event in disease pathogenesis: decreasing the levels of the disease-causing protein. Genetic data in humans and animal models provide evidence that increased levels of either the mutant or the normal proteins are at the root of the pathogenesis of several neurodegenerative diseases. For example, expanded polyglutamine tracts stabilize the disease proteins in Huntington's disease and spinocerebellar ataxias[41–43], whereas increased levels of wild-type APP and α-synuclein due to genomic duplications and triplications cause Alzheimer's and Parkinson's disease, respectively[9–11]. Therefore, targeting an early event in pathogenesis could potentially delay the disease onset for this class of disorders. Indeed, a key challenge in Alzheimer's and Parkinson's diseases has been our limited understanding of how the stability of APP and α-synuclein is controlled. An unbiased forward genetic screen using independent and complementary assays to decrease the levels of APP and α-synuclein is likely to yield a variety of targets that might change the landscape of therapeutic development for these diseases. Furthermore, applying this approach at a genome-wide scale would enable us to discover other possible therapeutic targets. We note that cross-species comparative genomics (messenger RNA expression profiling and gene copy number) have

been recently used to discover new pathogenic pathways in the cancer field[44]. We believe that this study provides a proof-of-principle for addressing other neurodegenerative diseases using a similar conceptual strategy.

METHODS

Generation of stable cell lines

mRFP–ATXN1(82Q)–IRES–YFP was cloned into pHAGE vector. Lentiviral packaged clones were infected into Daoy cells and then were selected with puromycin and ran through Aria II (BD Biosciences) for selection of cells that shows expressions of mRFP and YFP. Other cell clones were generated by the same method: Daoy mRFP–ATXN1(30Q)–IRES–YFP and Daoy mRFP–IRES–YFP.

Cell-based kinase siRNA screen

Daoy mRFP–ATXN1(82Q)–IRES–YFP was split into 96-well plates. On the next day, each siRNA (kinase siRNA library from Invitrogen) was transfected at 20 nM with 0.08 μl of transfection reagent (Dharmacon) into corresponding wells and incubated for 72 h. Before running FACS analysis (LSR II, BD Biosciences), the cells were trypsinized and suspended in PBS with 5% FBS.

Drosophila kinase screen

For the screen we used the previously characterized *y,w,UAS-ATXN1(82Q)*(line-F7)*;GMR-GAL4* line[22] and for testing poly-glutamine specificity we used the *y,w,UAS-ATXN1(30Q)* (line-F1)*;GMR-GAL4*[22]. RNAi or loss-of-function alleles were obtained from the Vienna *Drosophila* RNAi Center (http://stockcenter.vdrc.at/control/main) and the Bloomington *Drosophila* Stock Center at University of Indiana (http://flystocks.bio.indiana.edu) repositories. Animals were crossed at 28 °C for external eye phenotype and 25 °C for retinal experiments. Scanning electron microscopy and paraffin sections of the retina were performed as previously described[22].

Cell culture and siRNA transfections

Daoy stable cell lines and Neuro2a cell lines were cultured in DMEM (Invitrogen) with 10% FBS (Invitrogen). siRNAs (Invitrogen) were transfected with DharmaFECT (Dharmacon) and incubated for 3 days before analysis. GST-fused human ATXN1(82Q) and ATXN1(82Q, S776A)[48], and Myc-fused mouse Msk1 (Open Biosystems), MEK-DD (gift of W. Hahn, Addgene plasmid no. 15268) and HRAS V12 (gift of W. Hahn, Addgene plasmid no. 9051) were transfected by Lipofectamine 2000 (Invitrogen). Inhibitors used: PD184352 (Santa Cruz Bio-technology), GW5074 (Sigma), H89 (Sigma) and Ro-31-8220 (Calbiochem).

Cell lysate preparation and immunoblot analysis

Before collection, cells were washed with PBS and lysed on ice for 20 min in radioimmunoprecipitation assay (RIPA) buffer (50 mM Tris-HCl, pH 7.6, 150 mM NaCl, 0.1% SDS, 0.5% sodium deoxycholate, 1% NP-40) supplemented with protease inhibitors

(Roche). The cell lysates were centrifuged at 15,000 g for 20 min at 4 °C, and the supernatants were analysed by SDS– PAGE and western blot. Primary antibodies used: anti-ATXN1 (11750), anti-pS776 ATXN1 (PN1248)[20], anti-GFP (Genetex), anti-Myc (Sigma), anti-GST (Sigma), anti-Gapdh (Advanced ImmunoChemical), anti-MEK (BD Biosciences), anti-Ras (BD Biosciences), anti-tubulin (Abcam) and anti-MSK1 (R&D Systems).

Kinase assay

Complementary DNAs of *ATXN1(82Q)* and *ATXN1(30Q)* were cloned into pDEST15 vector (GST-tagged, Invitrogen), and then transformed into BL21. GST–ATXN1(82Q) and GST–ATXN1(30Q) was purified through GST column. One microgram of GST–ATXN1(82Q) or (30Q) and 100 ng of active MSK1 (Invitrogen), RSK1 (Sigma) or RSK2 (Sigma) were incubated in kinase reaction buffer (50 mM Tris-HCl, pH 7.6, 150 mM NaCl, 10 mM $MgCl_2$, 1 mM dithiothreitol (DTT)) with phosphatase inhibitor (Roche) and 30 μM ATP (Invitrogen) for 30 min at 30 °C. The kinase reaction was terminated by adding both NuPAGE LDS sample buffer (Invitrogen) and sample reducing agent (Invitrogen) and then boiled for 10 min. The samples were run immediately onto NuPAGE Novex 4–12% Bis-Tris Gel (Invitrogen) for western blot analysis. Antibodies used were anti-ATXN1 (11750), anti-pS776 ATXN1 (PN1248)[20], anti-pan RSK1/2/3 (Cell Signaling Technology) and anti-MSK1 (R&D Systems).

Drosophila motor performance tests

Motor performance tests were done as previously described[28] with some modifications. Fifteen age-matched virgin females were placed in a vial and tapped down. The number of flies that climbed up 9 cm in 15 s was recorded. We repeated this ten consecutive times and the average of the ten observations was plotted for each day as shown in the chart. Two replicates were tested in parallel for each genotype. ATXN1(82Q) was expressed in the nervous system using *nrv2*-Gal4 (*y,w,UAS-ATXN1(82Q)(F7) nrv2-GAL4*).

Preparation of *Drosophila* protein lysates and immunoblot

Protein lysates were prepared in NuPAGE LDS sample buffer (Invitrogen), immunoblotted in acrylamide gels following standard procedures. Primary antibodies used are 11NQ anti-ATXN1 (Neuromab) and anti-laminC (Developmental Studies Hybridoma Bank).

Mouse brain slice culture

Mouse cerebella at postnatal day 11 were embedded in a 2% agarose GBSSK solution and sectioned at 350 μm as described[45]. Slices were cultured in collagen coated membrane inserts in cerebellar slice culture media. Half media changes were performed every 2–3 days, and PD184352 and Ro-31-8220 drugs were replaced accordingly.

Immunodepletion study

Dissected cerebella from FVB mice were homogenized in 100 μl lysis buffer (50 mM Tris, pH 7.5, 100 mM NaCl, 2.5 mM $MgCl_2$, 0.5% Triton X-100) containing protease inhibitor cocktail (Roche Biochemicals) and phosphatase inhibitor cocktails II and III (Sigma). Homogenates were frozen and thawed three times and cleared at 15,000 r.p.m. for 10 min.

For the immunodepletion, 150 μg of cleared cerebellar lysate was combined with 10 μl of PBS or goat anti-MSK1 antibody (R&D Systems, AF2518) and lysis buffer in a total volume of 100 μl for a minimum of 24 h at 4 °C with rotation. Fifty microlitres of a 50% slurry of Protein G Sepharose beads (Sigma) were added to the samples for a minimum of 48 h with regular rotation at 4 °C. Complete immunodepletion of the lysates was assessed by western blotting of the cleared lysates and proteins bound to the beads by boiling the beads in reducing sample buffer. Ten micrograms of mock- or kinase-depleted samples were combined with 10 mM $MgCl_2$ and 300 ng of GST-tagged ATXN1(30Q) protein; kinase reactions were initiated with the addition of 200 mM ATP followed by incubation at 30 °C for 0, 10, 30 or 60 min. Activity was stopped by boiling in Laemmli sample buffer for 10 min. Phosphorylation was quantified by western blot as previously described[29]. Data from five kinase assays from each set of immunodepletions was plotted, and statistical significance was determined using a Student's *t*-test.

Statistical analyses

To identify the primary screen hits, we calculated the whole-screen mean and selected the siRNAs that decreased the mRFP–ATXN1(82Q)/YFP ratio below 2 standard deviations. For the confirmation screen, we performed three independent experimental sets and compared the effect of siRNAs within each set to the internal siRNA controls by analysis of variance followed by Dunnet's and Tukey's post-hoc tests to select for the siRNAs that were significantly decreased. The same method was used to identify the false-positive siRNAs, by testing their effect on the control reporter mRFP–IRES–YFP cell line. All statistical analyses were performed using the JMP software from SAS.

Quantitative RT–PCR

RNA from siRNA-transfected Daoy (82Q) stable cells was extracted using Trizol (Invitrogen). Random-primed cDNA was obtained using the Superscript III kit (Invitrogen). Quantitative RT– PCR was performed using Perfecta SYBR Green FastMix (Quanta Biosciences). Primers used were as follows: FNTA: forward primer 5′-TGGACGACGGGTTTGTGAG-3′, reverse primer 5′-ACCGGATCTATATCAGCCCATT-3′; MEK2: forward 5′-CCAAGGTCGGCGAACTCAAA-3′, reverse 5′-TCTCAAGGTGGATCAGCTTCC-3′; MEK3: forward 5′-GTCGACTGTTTCTACACTGTC-3′, reverse 5′-GGATGTCCTCTGGAATTGTC-3′. siRNAs (Invitrogen) used were as follows: IGF1R_si1: sense 5′-UCUUCAAGGGCAAUUUGCUCAUUAA-3′, antisense 5′-UUAAUGAGCAAAUUGCCCUUGAAGA-3′; IGF1R_si2: sense 5′-CAACACUGGUCAUCAUGGAACUGAU-3′, antisense 5′-AUCAGUUCCAUGAUGACCAGUGUUG-3′; ULK3_si1: sense 5′-GGGACAGUGACAAUAUCUACCUCAU-3′, antisense 5′-AUGAGGUAGAUAUUGUCACUGUCCC-3′; ULK3_si2: sense 5′-UCGCUUCAUCCAUACCCGCAGGAUU-3′, antisense 5′-AAUCCUGCGGGUAUGGAUGAAGCGA-3′; WNK4_si1: sense 5′-UGGGCUUGGUCUGUGAAGCCGAUUA-3′, antisense 5′-UAAUCGGCUUCACAGACCAAGCCCA-3′; WNK4_si2: sense 5′-GCGAAAGCGUGAGAAGCUGCGUAAA-3′, antisense 5′-

UUUACGCAGCUUCUCACGCUUUCGC-3′; BUB1_si: sense 5′-GCUGCACAACUUGCGUCUACACCAU-3′, antisense 5′-AUGGUGUAGACGCAAGUUGUGCAGC-3′; MSK1_si1: sense 5′-UCCUUUGUUGCUCCUUCCAUCCUAU-3′, antisense 5′-AUAGGAUGGAAGGAGCAACAAAGGA-3′; MSK1_si2: sense 5′-CCUUUGUUGCUCCUUCCAUCCUAUU-3′, antisense 5′-AAUAGGAUGGAAGGAGCAACAAAGG-3′; MEK2_si: sense 5′-CGACUUCCAGGAGUUUGUCAAUAAA-3′, antisense 5′-UUUAUUGACAAACUCCUGGAAGUCG-3′; MEK3_si: sense 5′-CCUUCAUCACCAUUGGAGACAGAAA-3′, antisense 5′-UUUCUGUCUCCAAUGGUGAUGAAGG-3′; MEK6_si: sense 5′-CGGCUACUGAUGGAUUUGGAUAUUU-3′, antisense 5′-AAAUAUCCAAAUCCAUCAGUAGCCG-3′; ERK1_si: 5′-CCCUGGAAGCCAUGAGAGAUGUCUA-3′, antisense 5′-UAGACAUCUCUCAUGGCUUCCAGGG-3′; ERK2_si1: sense 5′-GCCGAAGCACCAUUCAAGUUCGACA-3′, antisense 5′-UGUCGAACUUGAAUGGUGCUUCGGC-3′; ERK2_si2: sense 5′-CCGAAGCACCAUUCAAGUUCGACAU-3′, antisense 5′-AUGUCGAACUUGAAUGGUGCUUCGG-3′; HRAS_si1: sense 5′-CCAUCCAGCUGAUCCAGAACCAUUU-3′, antisense 5′-AAAUGGUUCUGGAUCAGCUGGAUGG-3′; HRAS_si2: sense 5′-GAUCAAACGGGUGAAGGACUCGGAU-3′, antisense 5′-AUCCGAGUCCUUCACCCGUUUGAUC-3′; FNTA_si1: sense 5′-GCAGGAUCGUGGUCUUUCCAAAUAU-3′, antisense 5′-AUAUUUGGAAAGACCACGAUCCUGC-3′; FNTA_si2: sense 5′-GACAAUGGGUUAUUCAGGAAUUUAA-3′, antisense 5′-UUAAAUUCCUGAAUAACCCAUUGUC; FNTA_si3: sense 5′-CAUAAUGAAAGUGCAUGGAACUAUU-3′, antisense 5′-AAUAGUUCCAUGCACUUUCAUUAUG-3′.

Mouse models

All procedures for mouse animal use were approved by the Institutional Animal Care and Use Committee for Baylor College of Medicine and Affiliates. *Atxn1*$^{154Q/+}$ has been previously described[35] and has been backcrossed to C57BL/6 for more than ten generations. FVB *ATXN1(82Q) B05* transgenic[38] and C57BL/6 *Msk1*$^{-/-}$ *Msk2*$^{-/-}$[36,37] mice have been previously generated and characterized. Male *Atxn1*$^{154Q/+}$ animals were crossed with female *Msk1*$^{+/-}$ *Msk2*$^{+/-}$ to obtain the following genotypes: wild type, *Msk1*$^{+/-}$, *Msk2*$^{+/-}$, *Msk1*$^{+/-}$ *Msk2*$^{+/-}$, *Atxn1*$^{154Q/+}$, *Msk1*$^{+/-}$ *Atxn1*$^{154Q/+}$, *Msk2*$^{+/-}$ *Atxn1*$^{154Q/+}$ and *Msk1*$^{+/-}$ *Msk2*$^{+/-}$ *Atxn1*$^{154Q/+}$. Male *ATXN1(82Q)*(*B05*) was crossed with female *Msk1*$^{+/-}$ *Msk2*$^{+/-}$ for the following F_1 genotypes: wild type, *Msk1*$^{+/-}$, *Msk2*$^{+/-}$, *Msk1*$^{+/-}$ *Msk2*$^{+/-}$, *ATXN1(82Q)*(*B05*), *ATXN1(82Q)*(*B05*) *Msk1*$^{+/-}$, *ATXN1(82Q)(B05)* *Msk2*$^{+/-}$ and *ATXN1(82Q)*(*B05*) *Msk1*$^{+/-}$ *Msk2*$^{+/-}$.

Rotarod analysis

Rotarod analysis was performed as previously described[46], with four trials for 4 days using 9–10-week-old male mice. Data were analysed using post-hoc test.

Mouse brain lysate preparation and immunoblot analysis

Mice cerebella were dissected and then lysed in RIPA buffer (50 mM Tris-HCl, pH 7.6, 150 mM NaCl, 0.1% SDS, 0.5% sodium deoxycholate, 1% NP-40) supplemented with protease inhibitors (Roche). The protein lysate was then incubated on ice for 20 min and centrifuged at 13,000 r.p.m. for 20 min at 4 °C, and the supernatants were analysed by SDS–PAGE and western blot. Primary antibodies used were anti-ATXN1 (11750), anti-pS776 ATXN1 (PN1248)[20], anti-Gapdh (Advanced ImmunoChemical), anti-pERK (Cell signaling), anti-tubulin (Abcam) and anti-MSK1 (R&D Systems).

Purkinje cell pathology analysis

Mice were perfused with 4% paraformaldehyde in PBS and whole brains were dissected. Cerebellar sections were cut at a thickness of 30 μm and were immunostained with anti-calbindin antibody (Sigma) and imaged using a Zeiss LSM 710 confocal microscope. Quantitation was performed using ImageJ software as previously described[47]. Data were analysed using post-hoc test.

Drosophila lifespan assays

Two replicates of 30 female virgins each were aged at 26.5 °C. Vials were counted every day for the duration of the experiment to score dead animals. Data was represented using Kaplan–Meyer and significance was assessed through the Wilcoxon test.

Functional enrichment and network analysis of modifiers

Functional enrichment was assessed using KEGG/DAVID analysis database (http://david.abcc.ncifcrf.gov/). We carried out network analysis using Ingenuity Pathway Analysis and manual curation.

Gel-filtration chromatography and kinase assay

Protein lysates were prepared from two C57BL/6 wild-type mouse cerebellum and gel-filtration chromatography was performed as described previously[46,47]. Atxn1 carboxy-terminal fragment (the last 269 amino acids of Atxn1) fused to maltose binding protein (MBP) was purified from bacteria[49]. Kinase assay reactions were set up by combining 1% of each fractionated cerebellar lysate with 100 ng MBP–Atxn1 C-terminal fragment in kinase buffer (50 mM Tris-HCl, pH 7.6, 150 mM NaCl, 10 mM $MgCl_2$, 1 mM DTT) with phosphatase inhibitor (Roche) and 30 μM ATP (Invitrogen) and then were incubated for 30 min at 30 °C. The kinase reaction was terminated by adding NuPAGE LDS sample buffer (Invitrogen) and sample reducing agent (Invitrogen) and then boiled for 10 min. The samples were run immediately onto NuPAGE Novex 4–12% Bis-Tris Gel (Invitrogen) for western blot analysis. S776 phosphorylation was detected by using anti-pS776 ATXN1 antibody (PN1248)[20].

Supplementary Material

Refer to Web version on PubMed Central for supplementary material.

Acknowledgments

We thank the members of the Zoghbi, Botas, Orr and Westbrook laboratories for suggestions and discussions, and V. Brandt for editorial input. We also appreciate the help from CCSC and C-BASS cores at The Baylor College of Medicine (BCM) for FACS analysis and the confocal microscopy and mouse behavioural cores of the BCM Intellectual and Developmental Disabilities Research Center (HD024064). Thanks to J. Barrish at Texas Children's Hospital for help with scanning electron microscopy. This work was supported by a Howard Hughes Medical Institute Collaborative Innovation Awards grant.

References

1. Evans DA. Estimated prevalence of Alzheimer's disease in the United States. Milbank Q. 1990; 68:267–289. [PubMed: 2233632]
2. Hindle JV. Ageing, neurodegeneration and Parkinson's disease. Age Ageing. 2010; 39:156–161. [PubMed: 20051606]
3. Marsden CD, Parkes JD. Success and problems of long-term levodopa therapy in Parkinson's disease. Lancet. 1977; 1:345–349. [PubMed: 64868]
4. Scarpini E, Scheltens P, Feldman H. Treatment of Alzheimer's disease: current status and new perspectives. Lancet Neurol. 2003; 2:539–547. [PubMed: 12941576]
5. Ross CA, Poirier MA. Protein aggregation and neurodegenerative disease. Nature Med. 2004; 10:S10–S17. [PubMed: 15272267]
6. Taylor JP, Hardy J, Fischbeck KH. Toxic proteins in neurodegenerative disease. Science. 2002; 296:1991–1995. [PubMed: 12065827]
7. Haass C, Selkoe DJ. Soluble protein oligomers in neurodegeneration: lessons from the Alzheimer's amyloid β-peptide. Nature Rev. Mol. Cell Biol. 2007; 8:101–112. [PubMed: 17245412]
8. Zoghbi HY, Orr HT. Glutamine repeats and neurodegeneration. Annu. Rev. Neurosci. 2000; 23:217–247. [PubMed: 10845064]
9. Singleton AB, et al. α-synuclein locus triplication causes Parkinson's disease. Science. 2003; 302:841. [PubMed: 14593171]
10. Chartier-Harlin MC, et al. α-synuclein locus duplication as a cause of familial Parkinson's disease. Lancet. 2004; 364:1167–1169. [PubMed: 15451224]
11. Rovelet-Lecrux A, et al. APP locus duplication causes autosomal dominant early-onset Alzheimer disease with cerebral amyloid angiopathy. Nature Genet. 2006; 38:24–26. [PubMed: 16369530]
12. Götz J, Ittner LM. Animal models of Alzheimer's disease and frontotemporal dementia. Nature Rev. Neurosci. 2008; 9:532–544. [PubMed: 18568014]
13. Williams AJ, Paulson HL. Polyglutamine neurodegeneration: protein mis-folding revisited. Trends Neurosci. 2008; 31:521–528. [PubMed: 18778858]
14. Xia H, et al. RNAi suppresses polyglutamine-induced neurodegeneration in a model of spinocerebellar ataxia. Nature Med. 2004; 10:816–820. [PubMed: 15235598]
15. Harper SQ, et al. RNA interference improves motor and neuropathological abnormalities in a Huntington's disease mouse model. Proc. Natl Acad. Sci. USA. 2005; 102:5820–5825. [PubMed: 15811941]
16. Yamamoto A, Lucas JJ, Hen R. Reversal of neuropathology and motor dysfunction in a conditional model of Huntington's disease. Cell. 2000; 101:57–66. [PubMed: 10778856]
17. Zu T, et al. Recovery from polyglutamine-induced neurodegeneration in conditional *SCA1* transgenic mice. J. Neurosci. 2004; 24:8853–8861. [PubMed: 15470152]
18. Kordasiewicz HB, et al. Sustained therapeutic reversal of Huntington's disease by transient repression of huntingtin synthesis. Neuron. 2012; 74:1031–1044. [PubMed: 22726834]
19. Zoghbi HY, Orr HT. Pathogenic mechanisms of a polyglutamine-mediated neurodegenerative disease, spinocerebellar ataxia type 1. J. Biol. Chem. 2009; 284:7425–7429. [PubMed: 18957430]

20. Emamian ES, et al. Serine 776 of ataxin-1 is critical for polyglutamine-induced disease in *SCA1* transgenic mice. Neuron. 2003; 38:375–387. [PubMed: 12741986]
21. Noble ME, Endicott JA, Johnson LN. Protein kinase inhibitors: insights into drug design from structure. Science. 2004; 303:1800–1805. [PubMed: 15031492]
22. Fernandez-Funez P, et al. Identification of genes that modify ataxin-1-induced neurodegeneration. Nature. 2000; 408:101–106. [PubMed: 11081516]
23. Taniguchi CM, Emanuelli B, Kahn CR. Critial nodes in signalling pathways: insights into insulin action. Nature Rev. Mol. Cell Biol. 2006; 7:85–96. [PubMed: 16493415]
24. Shaharabany M, et al. Distinct pathways for the involvement of WNK4 in the signaling of hypertonicity and EGF. FEBS J. 2008; 275:1631–1642. [PubMed: 18312414]
25. Teixeira-Castro A, et al. Neuron-specific proteotoxicity of mutant ataxin-3 in *C. elegans*: rescue by the DAF-16 and HSF-1 pathways. Hum. Mol. Genet. 2011; 20:2996–3009. [PubMed: 21546381]
26. Cobb MH. MAP kinase pathways. Prog. Biophys. Mol. Biol. 1999; 71:479–500. [PubMed: 10354710]
27. Avruch J. Insulin signal transduction through protein kinase cascades. Mol. Cell. Biochem. 1998; 182:31–48. [PubMed: 9609112]
28. Al-Ramahi I, et al. dAtaxin-2 mediates expanded Ataxin-1-induced neurodegeneration in a *Drosophila* model of SCA1. PLoS Genet. 2007; 3:e234. [PubMed: 18166084]
29. Jorgensen ND, et al. Phosphorylation of ATXN1 at Ser776 in the cerebellum. J. Neurochem. 2009; 110:675–686. [PubMed: 19500214]
30. Roux PP, Blenis J. ERK and p38 MAPK-activated protein kinases: a family of protein kinases with diverse biological functions. Microbiol. Mol. Biol. Rev. 2004; 68:320–344. [PubMed: 15187187]
31. Mody N, Leitch J, Armstrong C, Dixon J, Cohen P. Effects of MAP kinase cascade inhibitors on the MKK5/ERK5 pathway. FEBS Lett. 2001; 502:21–24. [PubMed: 11478941]
32. Lackey K, et al. The discovery of potent cRaf1 kinase inhibitors. Bioorg. Med. Chem. Lett. 2000; 10:223–226. [PubMed: 10698440]
33. Deak M, Clifton AD, Lucocq LM, Alessi DR. Mitogen- and stress-activated protein kinase-1 (MSK1) is directly activated by MAPK and SAPK2/p38, and may mediate activation of CREB. EMBO J. 1998; 17:4426–4441. [PubMed: 9687510]
34. Lorenzetti D, et al. Repeat instability and motor incoordination in mice with a targeted expanded CAG repeat in the *Sca1* locus. Hum. Mol. Genet. 2000; 9:779–785. [PubMed: 10749985]
35. Watase K, et al. A long CAG repeat in the mouse *Sca1* locus replicates SCA1 features and reveals the impact of protein solubility on selective neurodegeneration. Neuron. 2002; 34:905–919. [PubMed: 12086639]
36. Arthur JS, Cohen P. MSK1 is required for CREB phosphorylation in response to mitogens in mouse embryonic stem cells. FEBS Lett. 2000; 482:44–48. [PubMed: 11018520]
37. Wiggin GR, et al. MSK1 and MSK2 are required for the mitogen- and stress-induced phosphorylation of CREB and ATF1 in fibroblasts. Mol. Cell. Biol. 2002; 22:2871–2881. [PubMed: 11909979]
38. Burright EN, et al. *SCA1* transgenic mice: a model for neurodegeneration caused by an expanded CAG trinucleotide repeat. Cell. 1995; 82:937–948. [PubMed: 7553854]
39. Dar AC, Das TK, Shokat KM, Cagan RL. Chemical genetic discovery of targets and anti-targets for cancer polypharmacology. Nature. 2012; 486:80–84. [PubMed: 22678283]
40. van Ham TJ, Breitling R, Swertz MA, Nollen EA. Neurodegenerative diseases: lessons from genome-wide screens in small model organisms. EMBO Mol. Med. 2009; 1:360–370. [PubMed: 20049741]
41. Jeong H, et al. Acetylation targets mutant huntingtin to autophagosomes for degradation. Cell. 2009; 137:60–72. [PubMed: 19345187]
42. Matsumoto M, et al. Molecular clearance of ataxin-3 is regulated by a mammalian E4. EMBO J. 2004; 23:659–669. [PubMed: 14749733]
43. Cummings CJ, et al. Mutation of the E6-AP ubiquitin ligase reduces nuclear inclusion frequency while accelerating polyglutamine-induced pathology in *SCA1* mice. Neuron. 1999; 24:879–892. [PubMed: 10624951]

44. Chin L, Gray JW. Translating insights from the cancer genome into clinical practice. Nature. 2008; 452:553–563. [PubMed: 18385729]
45. Falsig J, Aguzzi A. The prion organotypic slice culture assay—POSCA. Nature Protocols. 2008; 3:555–562.
46. Jafar-Nejad P, Ward CS, Richman R, Orr HT, Zoghbi HY. Regional rescue of spinocerebellar ataxia type 1 phenotypes by 14–3-3 haploinsufficiency in mice underscores complex pathogenicity in neurodegeneration. Proc. Natl Acad. Sci. USA. 2011; 108:2142–2147. [PubMed: 21245341]
47. Bowman AB, et al. Duplication of *Atxn1l* suppresses SCA1 neuropathology by decreasing incorporation of polyglutamine-expanded ataxin-1 into native complexes. Nature Genet. 2007; 39:373–379. [PubMed: 17322884]
48. Lim J, et al. Opposing effects of polyglutamine expansion on native protein complexes contribute to SCA1. Nature. 2008; 452:713–718. [PubMed: 18337722]
49. Servadio A, et al. Expression analysis of the ataxin-1 protein in tissues from normal and spinocerebellar ataxia type 1 individuals. Nature Genet. 1995; 10:94–98. [PubMed: 7647801]

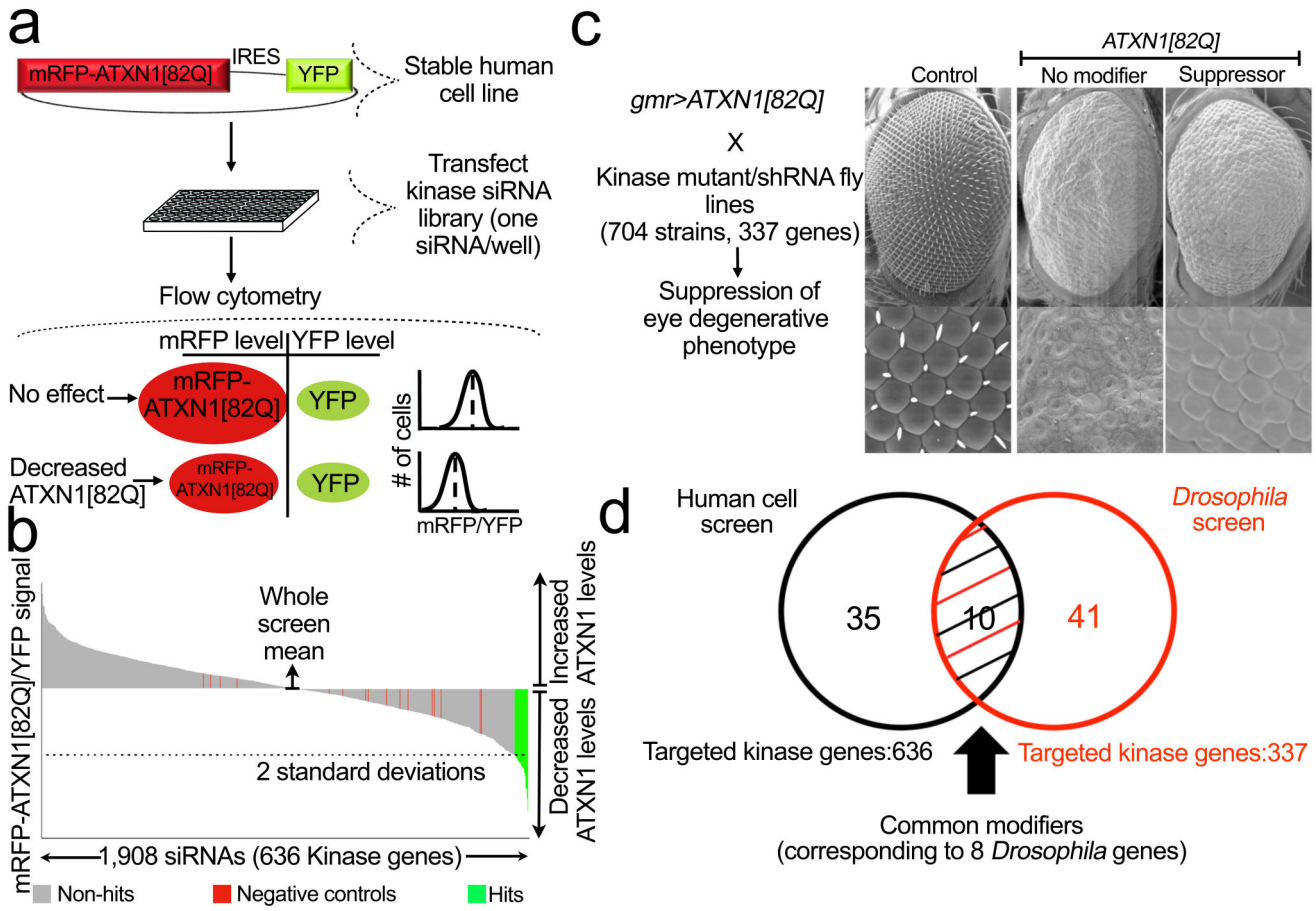

Figure 1. Integrative genetic screen identifies regulators of ATXN1(82Q) stability

a, Forward genetic screen strategy for modifiers of ATXN1(82Q) levels. mRFP–ATXN1(82Q)–IRES– YFP-expressing cells are used to assess the abundance of ATXN1(82Q) by monitoring the mRFP–ATXN1(82Q) to YFP fluorescence ratio. siRNAs that reduce ATXN1(82Q) protein lead to a decrease in mRFP–ATXN1(82Q) but not YFP. **b**, Primary screen result shows the effect on the average mRFP–ATXN1(82Q)/YFP ratio per kinase siRNAs tested. **c**, Schematic of the *Drosophila* screen for suppressors of ATXN1(82Q). Suppressor example is *lic* (homologue of human MEK3). **d**, Venn diagram of the identified gene candidates.

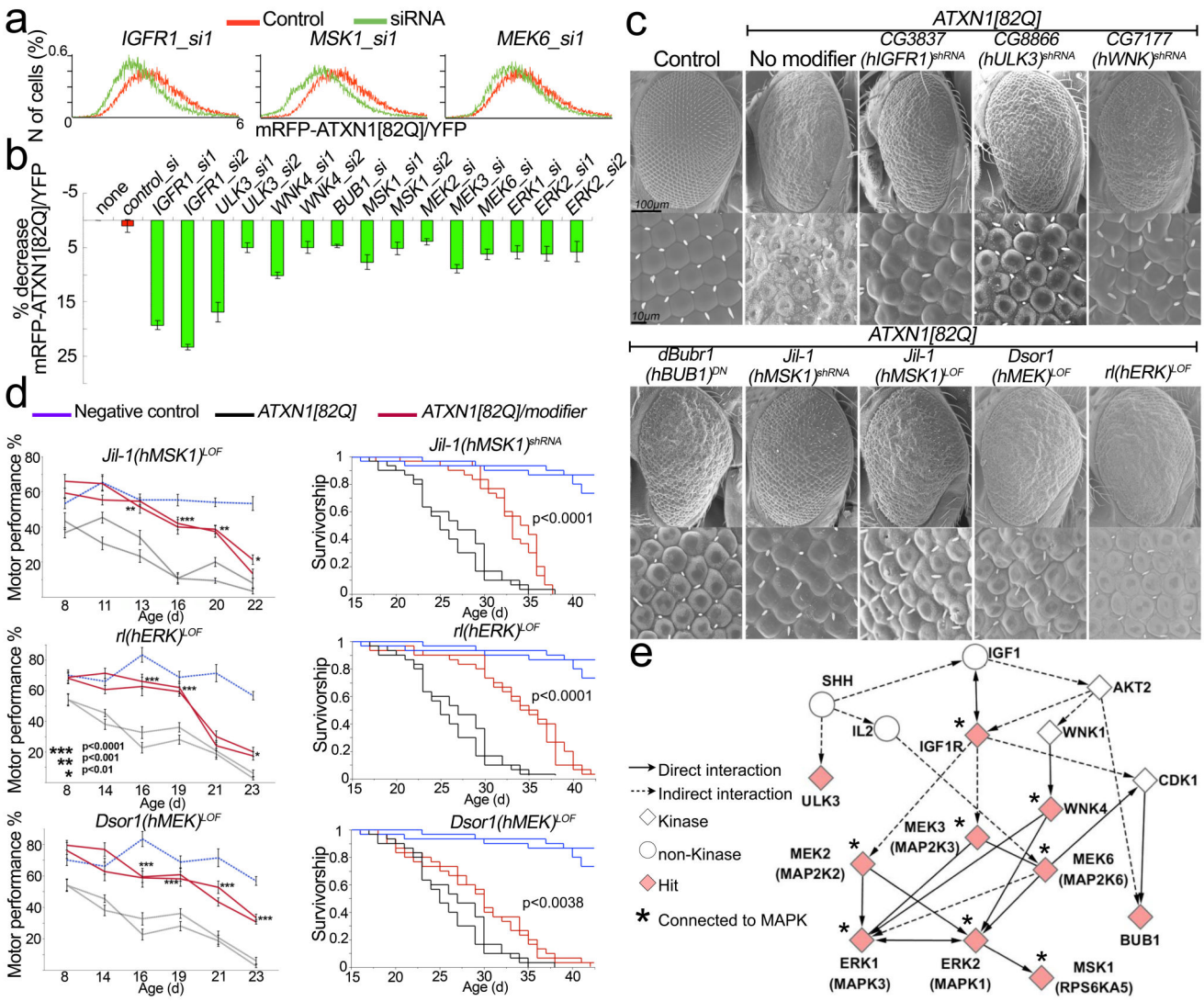

Figure 2. Modifiers shared between cell-based and *in vivo* screens

a, Histograms show the distribution of mRFP–ATXN1(82Q)/YFP ratio abundance in cells treated with indicated siRNA compared to control (*n*, number). **b**, Average mRFP–ATXN1(82Q)/YFP ratio change upon treatment with siRNAs hits (error bars: s.e.m. from triplicates, $P < 0.05$). **c**, Scanning electron microscopy (SEM) images of ATXN1(82Q) suppressors in *Drosophila* caused by reduced level of candidate genes in **b**. LOF, loss of function. DN, dominant negative. Names of human (h) homologues are noted in parentheses. **d**, Decreased levels of *Drosophila* MSK1, ERK and MEK homologues suppress motor impairment and improve survival. Error bars, s.e.m. **e**, Pathway analysis showing eight of the ten modifiers connected to MAPK pathway. Diamonds represent modifiers common to both screens.

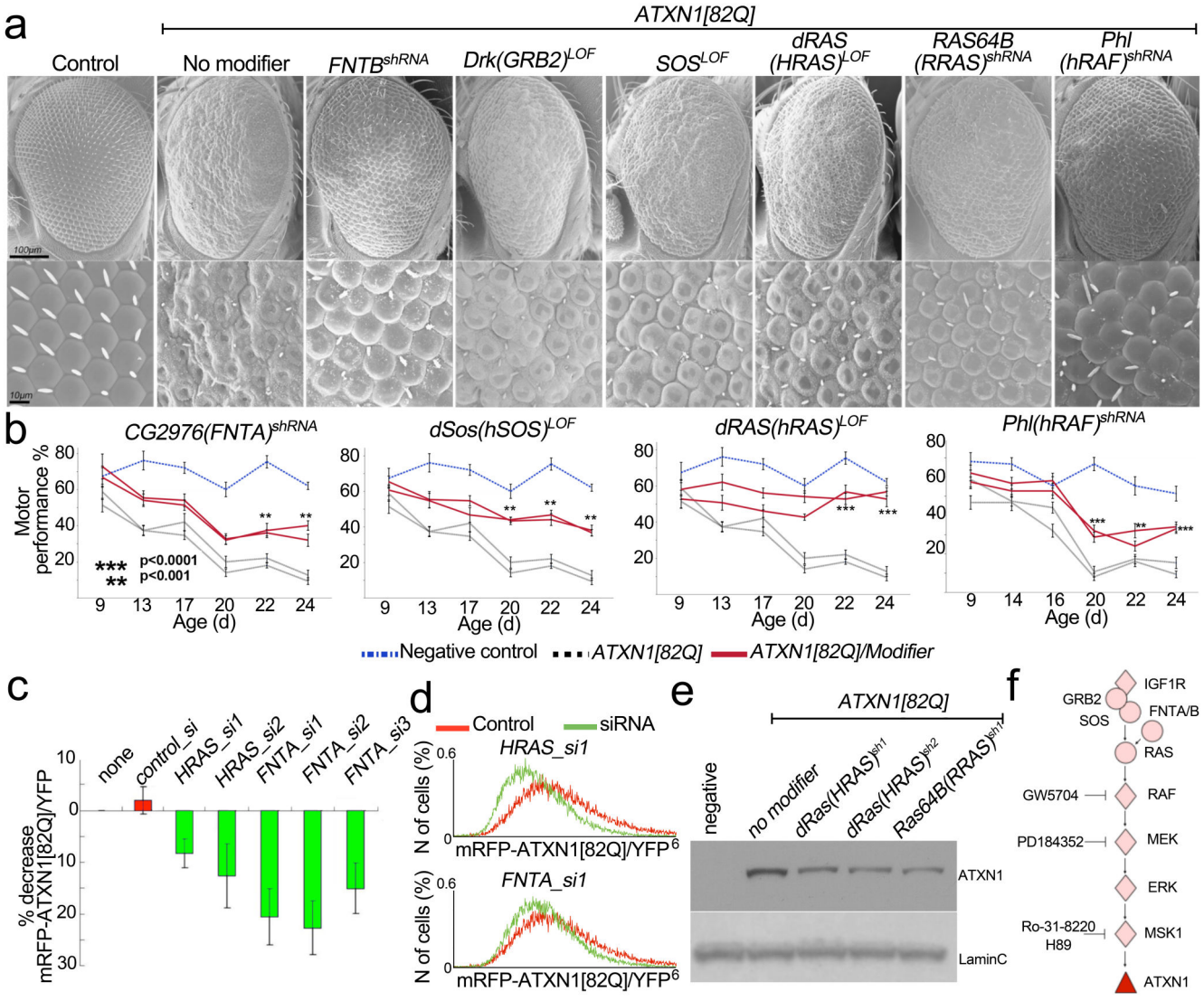

Figure 3. Upstream MAPK pathway components regulate ATXN1 toxicity and levels

a, Decreased levels of *Drosophila* homologues of the MAPK upstream components suppress ATXN1(82Q)-induced eye degeneration. **b**, Decreased levels in the *Drosophila* homologues of FNTA, SOS, HRAS and RAF suppress ATXN1(82Q)-induced motor impairments. **c**, Change in mRFP–ATXN1(82Q)/YFP average fluorescence ratio upon treatment with indicated siRNAs. Error bars, s.e.m. from triplicates, $P < 0.05$. **d**, mRFP–ATXN1(82Q)/YFP ratio distribution in siRNA-treated whole-cell populations compared to control. **e**, Decreased levels of ATXN1(82Q) induced by RAS shRNA in *Drosophila*. **f**, MAPK pathway showing the ATXN1(82Q) modifiers and Fig. 5 inhibitors. Diamonds represent modifiers from the screen.

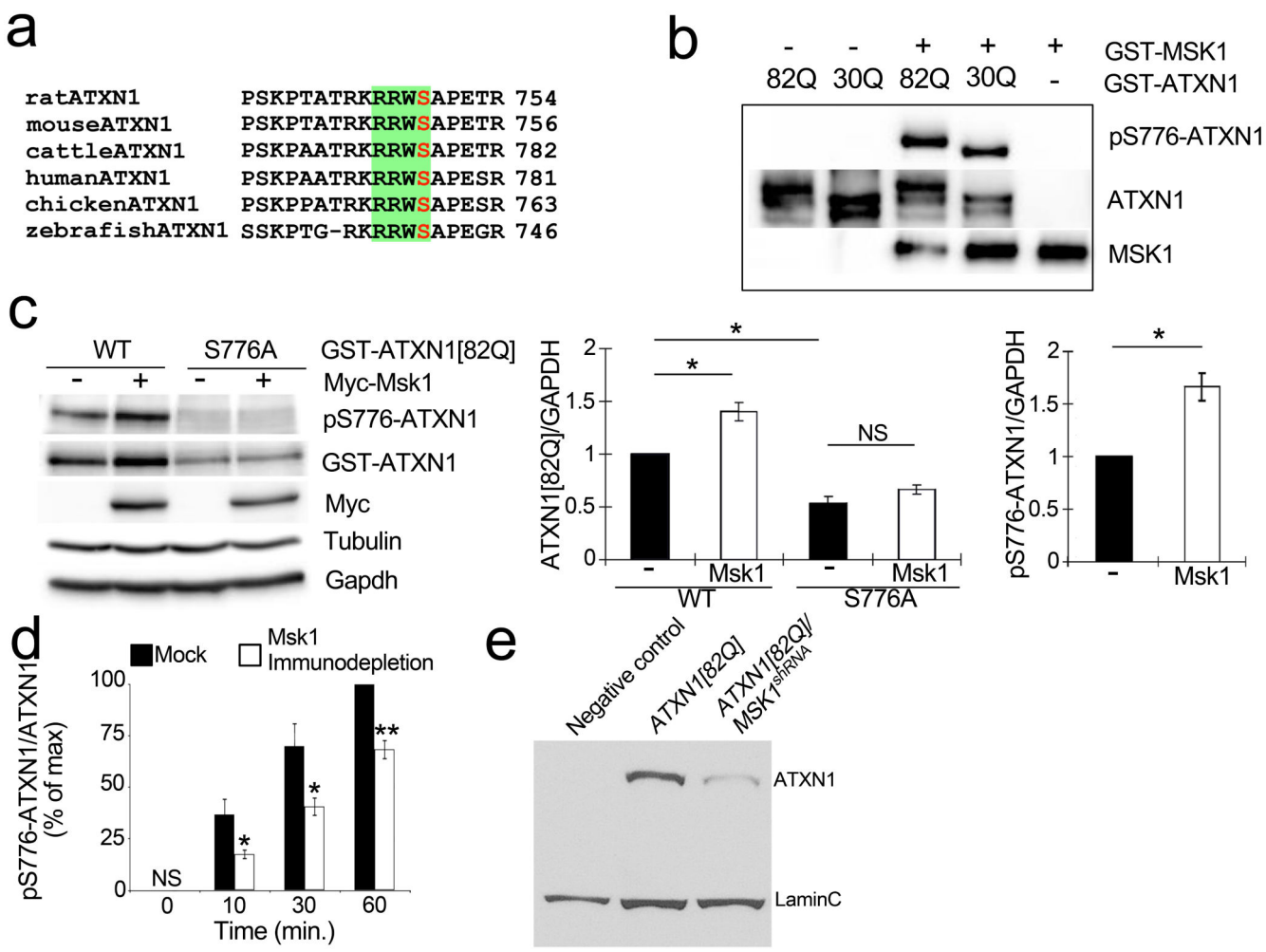

Figure 4. MSK1 phosphorylates ATXN1 at S776 and controls its stability

a, MSK1 phosphorylation consensus site, RXXS, found in ATXN1 across different species. **b**, *In vitro* kinase assay with purified GST–ATXN1(82Q) or GST–ATXN1(30Q) and GST–MSK1. **c**, Neuro2a western blot transfected with Myc-fused mouse Msk1 and GST–ATXN1(82Q) or ATXN1(82Q, S776A). Graphs (right) show signal quantification of the western blot (error bars denote s.e.m. from three independent experiments, **P* < 0.05). WT, wild type. **d**, Immunodepletion of Msk1 from cerebellar extracts decreases the level of phospho-S776 ATXN1.**P* < 0.05, ***P* < 0.01, Student's *t*-test. **e**, Western blot shows that knockdown of MSK1 decreases ATXN1(82Q) level in fly heads of indicated genotypes (LaminC; loading control).

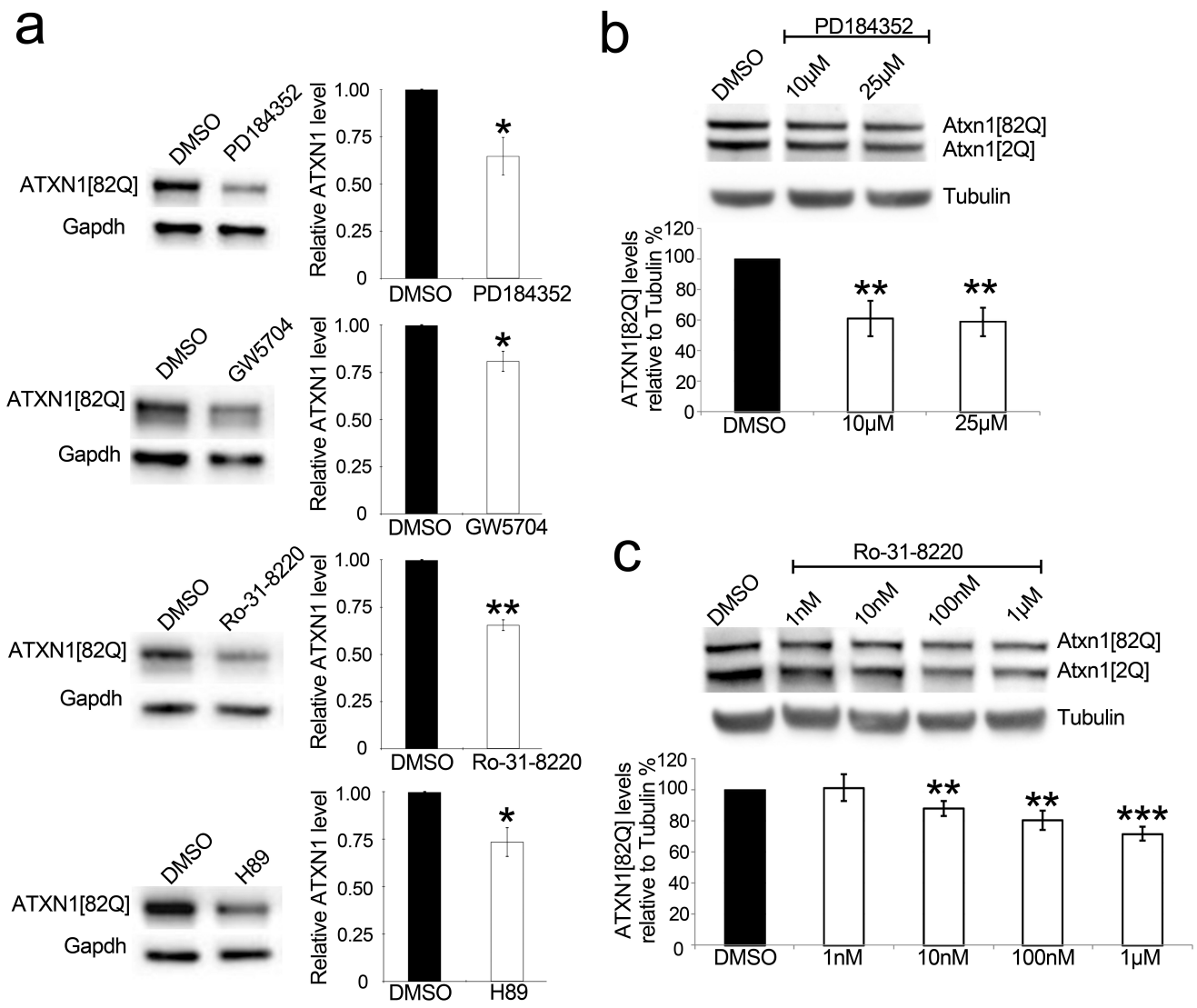

Figure 5. Pharmacological inhibition of the MAPK pathway decreases ATXN1 level

a, Western blots and quantifications show a decrease in ATXN1 levels from Daoy mRFP–ATXN1(82Q) cells upon treatment with the indicated inhibitors (PD184352, 10 μM; GW5704, 10 μM; Ro-31-8220, 1 μM; H89, 5 μM). Error bars indicate s.e.m. from three independent experiments. **b**, **c**, Dose–response graphs show a decrease in Atxn1 levels from mouse cerebellar slices upon treatment with the indicated inhibitors. Error bars indicate s.e.m. from three independent experiments. *$P < 0.05$, **$P < 0.01$, Student's *t*-test. DMSO, dimethylsulphoxide.

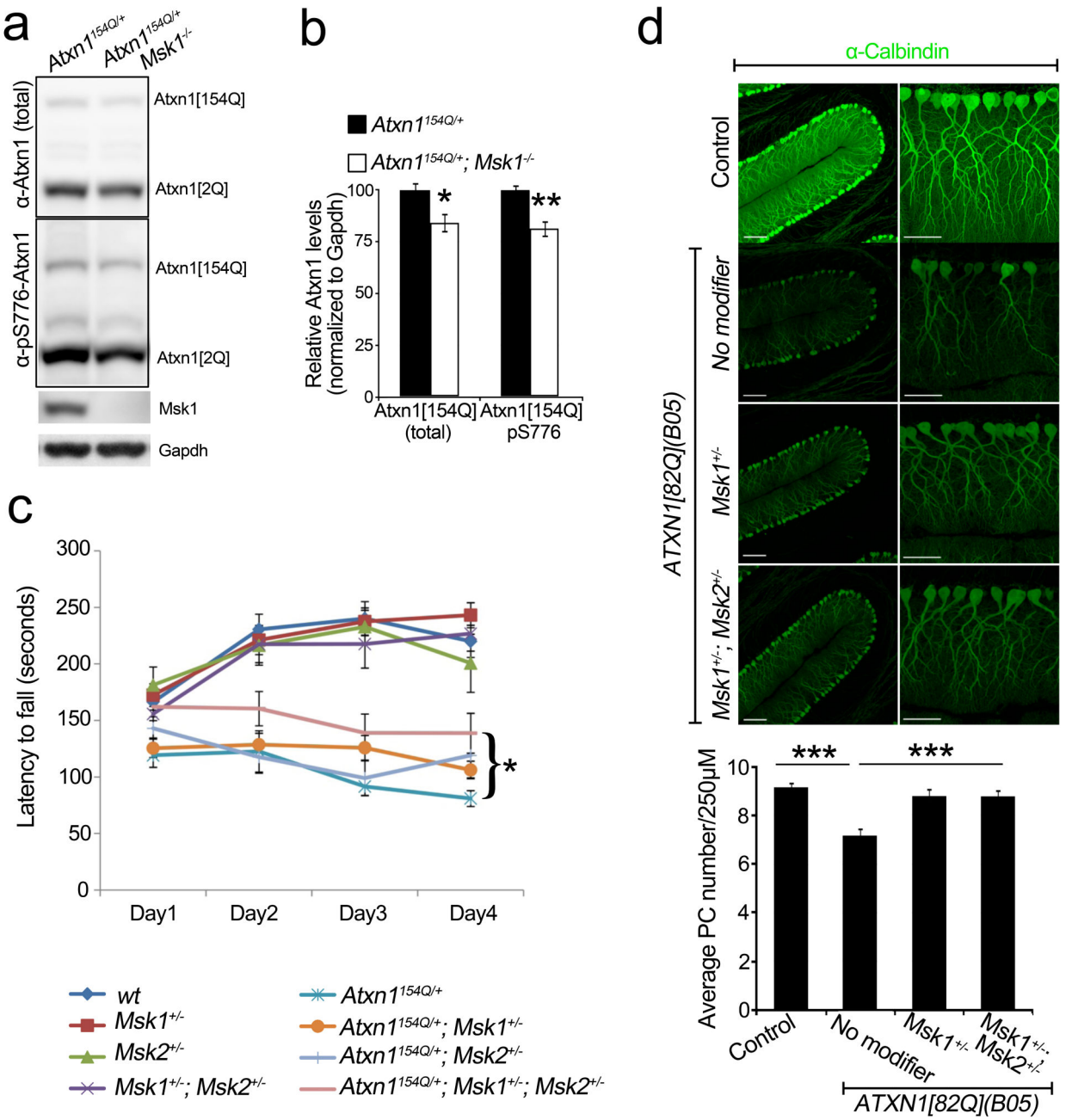

Figure 6. Msk reduction rescues behavioural and pathological phenotypes in SCA1 mice

a, **b**, Western blot and quantification show decreased Atxn1 levels in *Atxn1*$^{154Q/+}$ cerebella upon complete loss of Msk1 (4–5-week-old mice; error bars denote s.e.m. from $n = 4$ per genotype). **c**, Reduction of Msk1 and Msk2 improves motor performance of *Atxn1*$^{154Q/+}$ (9–10 weeks old, see Supplementary Information for details, $^*P = 0.027$). **d**, Partial loss-of-function of Msk1 alone or Msk1 and Msk2 rescues Purkinje cell (PC) loss of *ATXN1(82Q)*

(B05) mice (12 weeks old; $n = 3$ per genotype, three sections per mice). Scale bars, 100 μm (left), 50 μm (right). $*P < 0.05$, $**P < 0.01$, $***P < 0.001$, post-hoc Holm-Šídák test.